Biochemistry and Biophysics Reports 8 (2016) 184–191

Contents lists available at ScienceDirect

Biochemistry and Biophysics Reports

journal homepage: www.elsevier.com/locate/bbrep

# Human SLC26A4/Pendrin STAS domain is a nucleotide-binding protein: Refolding and characterization for structural studies

Alok K. Sharma [a,*], Tobias Krieger [a,b], Alan C. Rigby [c], Israel Zelikovic [d], Seth L. Alper [a,*]

[a] Division of Nephrology and Center for Vascular Biology Research, Beth Israel Deaconess Medical Center, Department of Medicine, Harvard Medical School, Boston, MA 02215, United States
[b] Paracelsus Medizinische Universitat, Salzburg, Austria
[c] Warp Drive Bio., Cambridge, MA 02139, United States
[d] Laboratory of Developmental Nephrology, Rambam Medical Center, and Department of Physiology and Biophysics, Faculty of Medicine, Technion, Haifa, Israel

ARTICLE INFO

*Article history:*
Received 6 June 2016
Received in revised form
28 July 2016
Accepted 23 August 2016
Available online 26 August 2016

*Keywords:*
SLC26A4
STAS domain
IVS
Protein refolding
NMR
Fluorescence

ABSTRACT

Mutations in the human SLC26A4/Pendrin polypeptide (hPDS) cause Pendred Syndrome /DFNB4, syndromic deafness with enlargement of the vestibular aqueduct and low-penetrance goiter. Here we present data on cloning, protein overexpression and purification, refolding, and biophysical characterization of the recombinant hPDS STAS domain lacking its intrinsic variable sequence (STAS-ΔIVS). We report a reproducible protein refolding protocol enabling milligram scale expression and purification of uniformly $^{15}N$- and $^{13}C/^{15}N$-enriched hPDS STAS-ΔIVS domain suitable for structural characterization by solution NMR. Circular dichroism, one-dimensional $^{1}H$, two-dimensional $^{1}H–^{15}N$ HSQC, and $^{1}H–^{13}C$ HSQC NMR spectra confirmed the well-folded state of purified hPDS STAS-ΔIVS in solution. Heteronuclear NMR chemical shift perturbation of select STAS-ΔIVS residues by GDP was observed at fast-to-intermediate NMR time scales. Intrinsic tryptophan fluorescence quench experiments demonstrated GDP binding to hPDS STAS-ΔIVS with $K_d$ of 178 μM. These results are useful for structure/function characterization of hPDS STAS, the cytoplasmic subdomain of the congenital deafness protein, pendrin, as well as for studies of other mammalian STAS domains.



## 1. Introduction

SLC26 family anion transport proteins are conserved throughout phylogeny from bacteria to humans [1,2]. In prokaryotes and plants this family of proteins is known as SulP (Sulfate Permease). SLC26 and SulP proteins consist of a short cytoplasmic N-terminus, a complex polytopic transmembrane domain of 14 trans-bilayer spans, and a cytoplasmic C-terminal region of 125–250 aa largely comprizing a Sulfate Transporter and anti-Sigma factor antagonist (STAS) domain [3]. The 10 known protein-coding human *SLC26* genes encode anion transporters, exchangers and channels expressed in epithelial cells and other cell types throughout the body. Mutations in at least four human SLC26 genes cause early-onset Mendelian diseases, including chondrodysplasia (SLC26A2/DTD), chloride-losing diarrhea (SLC26A3/DRA), deafness with enlargement of the vestibular aqueduct and low-penetrance goiter (SLC26A4/pendrin), and a rare form of impaired male fertility (SLC26A8). Many of these mutations involve the respective STAS domains. The human disease phenotypes are modeled in knockout mice with varying degrees of clinical fidelity, and genetic inactivation in mice of other *Slc26* genes unassociated as yet with human disease also causes pathogenic murine phenotypes. In addition, human SLC26A9 variants have been identified as strong risk modifiers of cystic fibrosis lung disease, whereas human pendrin (hPDS/SLC26A4) has been investigated as a risk modifier of systemic fluid balance, blood pressure, and asthma [2].

The STAS domains of SLC26/SulP transporters are homologous to bacterial anti-sigma factor antagonists such as SpoIIAA of *B. subtilis* [4,5]. Anti-sigma factor antagonists counter the activity of repressors (anti-sigma factors) of sigma (transcription) factors in the bacterial sporulation stress response pathway [6]. STAS domains are essential for plasmalemmal targeting, contribute to anion transport function and, like bacterial anti-sigma factors, serve as protein-protein interaction modules. Mutations in STAS domains of mammalian SLC26 transporters and bacterial SulP transporters impair function and/or surface expression of these transporters [3,7,8–10].

*Abbreviations:* hPDS, Human pendrin polypeptide; IVS, Intrinsic variable sequence; HSQC, Heteronuclear single quantum correlation spectroscopy; CD, Circular dichroism; MS, Mass spectroscopy

* Corresponding authors.
*E-mail addresses:* aksharma@bidmc.harvard.edu (A.K. Sharma), salper@bidmc.harvard.edu (S.L. Alper).

http://dx.doi.org/10.1016/j.bbrep.2016.08.022

SpoIIAA-like STAS domain structures solved by X-ray crystallography include those from dicarboxylate and bicarbonate transporter [11,12], DauA(YchM) of *E. coli* [13] and from dicarboxylate transporter SLC26Dg [3], as well as a STAS-ΔIVS structure from the cochlear outer hair cell Cl-dependent amplifier SLC26A5/prestin of rat [14]. NMR solution structures have been solved for rat prestin STAS-ΔIVS [14] and for the intact putative sulfate transporter Rv1739c of *M. tuberculosis* [15]. The presence of the unstructured "intervening sequence" (IVS) located between STAS helices α1 and β3 (nomenclature from [14]) distinguishes mammalian and metazoan STAS domains from those of bacterial anti-sigma factor antagonists and SulP transporters. No function has yet been reported for the IVS, and its deletion was required for protein overexpression and production of the first STAS domain crystals diffracting to high resolution [14]. All mammalian STAS domains reported subsequently have lacked the IVS, and along with bacterial STAS domains have yielded monomeric solution structures. Two-dimensional $^{1}H$–$^{15}N$ HSQC spectra of wildtype and mutant STAS from human SLC26A3/DRA have been presented without NMR assignment [8].

In addition to their enabling contributions to SLC26-mediated anion transport, SulP STAS domains are also nucleotide binding proteins [12,15], as previously demonstrated for SpoIIAA and ASAs [4,5]. Mammalian STAS domains have been shown to interact with multiple proteins in pulldown assays, including CFTR [8], OASTL (for *A. thaliana* Sultr1) [16] and IQGAP-1 [11]. Towards an understanding of the structural basis and functional utility of STAS domain nucleotide binding, we have initiated a structural characterization of the hPDS/SLC26A4 STAS domain by heteronuclear solution NMR, both in the absence and presence of the IVS. Here we present data on the molecular cloning, purification, and preliminary structural characterization of recombinant hPDS STAS domain lacking the IVS region (STAS-ΔIVS). The reported purification strategy yields well-folded hPDS STAS-ΔIVS in quantities and of stability sufficient for structural characterization by solution NMR. We also report biophysical experiments that demonstrate nucleotide binding by hPDS STAS-ΔIVS.

## 2. Materials and methods

### 2.1. Molecular cloning of recombinant hPDS STAS domain (ΔIVS)

To delimit operational boundaries of the STAS domain of SLC26A4/*hPDS* (Uniprot # O43511), the aa sequence of hPDS STAS was aligned with STAS domains of other human SLC26 polypeptides and with other structurally characterized STAS domains [5,17]. The secondary structure of hPDS STAS was predicted using Psipred (http://bioinf.cs.ucl.ac.uk/psipred/). These analyses suggested a STAS domain encompassing aa residues 517–734, with aa 575–652 as the IVS region. Initial hPDS STAS-ΔIVS constructs encompassing aa 512–780 ($hPDS_L$ STAS-ΔIVS) and aa 512–743 ($hPDS_S$ STAS-ΔIVS) were cloned in-frame into pET52b(+) (EMD Chemicals) with a C-terminal $His_{10}$-tag. A third STAS-ΔIVS construct encompassing aa 517–738 ($hPDS_{ST}$ STAS-ΔIVS) was cloned into pET28-a(+) in-frame with an N-terminal $His_6$-tag. Digested ligation products were transformed into *E. coli* BL21(DE3) cells (EMD chemicals). Plasmid sequence integrity was validated by DNA sequencing. Recombinant DNA was quantitated by Nanodrop spectrophotometer (Thermo Scientific, Waltham, MA), and DNA size and purity analyzed by 2% agarose gel.

### 2.2. Expression and isolation of purified hPDS STAS

*E.coli* BL21(DE3) cells harboring STAS-ΔIVS plasmids in pET52-b(+) and pET28-a(+) were grown overnight in LB medium containing kanamycin (30 μg/L). A 20 mL overnight inoculum was added to 2 L LB medium. Cultures were maintained at 37 °C until reaching OD 0.6–0.8. Protein expression was then induced by IPTG (empirically optimized at 750 μM) for 16 h at 13 °C. Induced cells were harvested by centrifugation (GSA rotor, Sorvall RC5B) at 6000 rpm for 15 min at 4 °C, and stored at −80 °C until further use. Harvested cells were freeze–thawed and suspended in buffer A (25 mM Tris-HCl, pH 8.5, 150 mM NaCl, 10 mM imidazole) supplemented with complete protease inhibitor cocktail tablet (Roche), 0.01% PMSF, and lysonase (Novagen) (10 μl/l cell culture), then agitated 30 min at 4 °C, and sonicated (Branson digital sonifier, S-450D) at 4 °C, 7 × 7 s cycles at 35% amplitude with 1 min on ice between cycles.

### 2.3. Purification of insoluble STAS-ΔIVS polypeptide

Lysate was centrifuged 30 min at 17,000 rpm at 4 °C to separate soluble and insoluble (inclusion body-containing) fractions. SDS-PAGE of preparations from all three STAS-ΔIVS constructs revealed that each accumulated predominantly in inclusion bodies which were washed 3x in buffer A and solubilized in buffer A containing 6 M Guanidine HCl. The cleared, denatured lysate was loaded onto pre-equilibrated Ni-NTA columns (Qiagen). STAS-ΔIVS protein was purified as previously described for Rv1739c STAS [18], except for inclusion of 2 M urea in wash and elution buffers, and additional modifications described in Supplementary Information. Eluate fractions were evaluated by SDS-PAGE. STAS-ΔIVS-containing fractions were pooled and dialyzed in refolding buffer B (25 mM Tris-HCl, 50 mM NaCl, pH 7.9) at 4 °C with three buffer replacements at 12 h intervals. The dialyzed STAS-ΔIVS protein was subsequently purified by anion-exchange chromatography (Q-sepharose fast flow matrix, GE Healthcare, Marlborough, MA). Purified protein was eluted in buffer B with a salt gradient increasing to 1 M NaCl. Q-sepharose eluates were dialyzed in buffer C (25 mM Tris-HCl, 150 mM NaCl, pH 7.9).

Immunoblot analysis was performed with mouse monoclonal anti-$(His)_6$ antibody (Sigma-Aldrich, EMDMillipore, Billerica, MA) diluted 1:3000. HRP-conjugated secondary antibodies (Sigma-Aldrich) were diluted 1:1000. Proteins were separated on 16% SDS-PAGE. ECL signal was detected with reagents from Amersham Biosciences by Kodak X-omat 2000 A.

Protein purification was assessed by size exclusion chromatography using a Biologic Duo flow FPLC system (Bio-Rad) at 4 °C on a Superdex 75 column (Amersham Biosciences) of 125 mL bed volume at 1 mL/min flow-rate, pre-calibrated with molecular weight standards (Bio-Rad) and pre-equilibrated in buffer C.

For expression of $^{15}N$-enriched protein constructs, *E.coli* BL21 (DE3) cells harboring $hPDS_{ST}$ STAS-ΔIVS plasmid in PET28-a(+) were grown in M9 minimal media containing $^{15}NH_4Cl$ (1 g/l), $^{12}C$-glucose (2 g/l) (Cambridge Isotope Laboratories; CIL) supplemented with 10 mL/L Bioexpress cell growth media (U-$^{15}N$, 98%; 10x concentrate, CIL) as sole carbon and nitrogen sources. $^{13}C/^{15}N$-enriched STAS-ΔIVS proteins were produced using $^{15}NH_4Cl$ (1 g/l), $^{13}C$-glucose (2 g/l), and U-$^{15}N$, $^{13}C$ (98%, 10x concentrate. CIL). Purification of $^{15}N$ or $^{13}C/^{15}N$-enriched $hPDS_{ST}$ STAS-ΔIVS was conducted by methods identical to those used for unlabeled protein. The $His_6$-tag was removed by thrombin cleavage (GE Healthcare; 2U/mg, 16 h at 4 °C), then quenched by 1 mM PMSF. Tag-free $hPDS_{ST}$ STAS-ΔIVS protein was recovered from repassing the cleaved reaction mixture through freshly prepared, buffer B-equilibrated Ni-NTA beads. For solution NMR experiments, samples additionally purified by anion exchange chromatography were dialyzed in Buffer D (40 mM potassium phosphate, 150 mM NaCl, pH 6.25). Purified $hPDS_{ST}$ STAS-ΔIVS samples were stable at pH 6.2, allowing collection of high quality heteronuclear NMR data of good signal-to-noise ratio. Purified STAS-ΔIVS protein was

concentrated with Millipore stirred cell membranes or with Amicon 10 kDa NMWL membrane centrifugal devices (Millipore), then quantitated by Bradford assay [19].

### 2.4. MALDI-TOF MS

$hPDS_{ST}$ STAS-ΔIVS protein identity and homogeneity were tested by MALDI-TOF MS by determination of the *m/z* ratio on an AB/MDS Sciex 4800 Plus MALDI TOF/TOF Analyzer (Applied Biosystems, Carlsbad, CA). $His_6$-tagged protein was diluted 1:20 into a solution of standard MALDI matrix sinapinic acid (prepared from 5.0 mg/mL stock), spotted onto the 4800 OptiTOF metal target plate and dried. Data were collected as total ion current (TIC) from 500 laser shots.

### 2.5. CD spectroscopy

Protein folding and intrinsic secondary structural characteristics of recombinant $hPDS_{ST}$ STAS-ΔIVS domain were assessed by Far-UV (260–190 nm) CD measurements at 25 °C on a Jasco-810 spectropolarimeter (Tufts University School of Medicine, Boston, MA). Anion exchange chromatography-purified and Buffer C-dialyzed sample was used for CD analysis. Prior to data collection, protein samples were clarified by centrifugation at 13,000 rpm, 1 min, 4 °C (Eppendorf 5424 R). Data were collected using a 1 mm path length quartz cuvette (Starna Cells, Atascadero, CA) with 1 nm bandwidth, 2 s response time, 20 nm/min scan speed, and 4 scans in continuous mode. Buffer-corrected spectra were recorded for 23 μM STAS-ΔIVS. Data were converted into Molar Residue Ellipticity (MRE) in units of θ (deg $cm^2$ $dmol^{-1}$) and analyzed using the program K2D2 [20]. Data were collected in triplicate and averaged for analysis.

### 2.6. Solution NMR spectroscopy

One-dimensional $^1H$, 2D $^1H$–$^{15}N$ HSQC [21] and $^1H$–$^{13}C$ HSQC (*constant time* t1 evolution) [22] NMR experiments were performed at 27 °C on a Bruker Avance spectrometer operating at $^1H$ frequency 600.133 MHz equipped with a 5 mm triple resonance (z-axis) pulsed-field gradient probe. NMR samples of $^{15}N$ or $^{13}C/^{15}N$-enriched STAS domains (0.25 mM) contained 10% (v/v) $D_2O$, 1 mM DTT-$d_{10}$, 0.25 mM DSS as internal standard, 0.05% (w/v) $NaN_3$, and 1X protease inhibitor. One dimensional $^1H$ NMR spectrum was acquired using a *zgcppr* pulse sequence with a *presaturation* scheme for water suppression employing a composite pulse. 512 scans were collected for 1D $^1H$ NMR data interpretation. 2D $^1H$–$^{15}N$ HSQC spectra were acquired using a relaxation delay of 1.00 s, with 8 scans (39 min acquizition time), 32 scans (2 h 45 min acquizition time) or 128 scans (10.3 h acquizition time). The 2D $^1H$–$^{13}C$ HSQC spectrum was acquired using the Echo-AntiEcho mode of quadrature detection ($^{13}C$ dimension), with respective spectral widths of 13 ppm and 80 ppm in $^1H$ and $^{13}C$ dimensions. Data were processed on an Intel PC workstation running OpenSuse11.1 using NMRPipe/NMRDraw processing software [23]. A Gaussian filter with a line-broadening parameter of 12 Hz was applied in direct and indirect acquired dimensions. All data sets were zero-filled once in each dimension to yield a final matrix of 2048*256 real data points. All $^1H$ chemical shift values were referenced with respect to internal standard DSS [24]. NMR data were analyzed with NMRDraw [23] and CCPNMR [25]. The $hPDS_{ST}$ STAS-ΔIVS interaction with GDP nucleotide was measured by collecting a series of 2D $^1H$–$^{15}N$ HSQC experiments of 32 scans. $hPDS_{ST}$ STAS-ΔIVS (0.25 mM) was titrated with nucleotide to a saturating concentration of 20 mM.

### 2.7. Fluorescence spectroscopy

One native Trp and six native Tyr residues of $hPDS_{ST}$ STAS-ΔIVS served as intrinsic fluorescence intensity probes. STAS protein purified by Ni-affinity- and anion exchange chromatography was used in Buffer C for fluorescence experiments. Samples were centrifuged before use. GDP free acid (Sigma) of highest available purity was prepared as stock solutions in buffer A. $hPDS_{ST}$ STAS-ΔIVS (20–23 μM; initial volume 200 mL) was preincubated in 48-well plates at 24 °C with nucleotide. Steady-state intrinsic fluorescence intensity of $hPDS_{ST}$ STAS-ΔIVS was then recorded at $\lambda_{em}$ 290–400 nm at 2-nm intervals with fixed $\lambda_{ex}$ 280 nm (SpectraMax M5, Molecular Devices, Sunnyvale, CA) in the presence of sequentially increasing nucleotide concentration, or titrated with buffer C alone. Protein and ligand were mixed and agitated 15 min prior to data collection. $hPDS_{ST}$ STAS-ΔIVS fluorescence at each nucleotide concentration was corrected for dilution and for inner filter effect (IFE) contributions of added nucleotide, on the intrinsic fluorescence of a mixture of a free tryptophan plus 6 M eq of free tyrosine (the 1:6 Trp: Tyr molar ratio reflected in the native $hPDS_{ST}$ STAS-ΔIVS aa sequence), with identical data acquizition parameters and instrument settings, as described [26]. IFE corrected and normalized fluorescence intensities were plotted as a function of nucleotide concentration and fit (SigmaPlot, Systat) to a single site ligand-binding model to determine dissociation constant ($K_d$) as described for nucleotide binding by Rv1739c STAS [15].

## 3. Results and discussion

### 3.1. Molecular cloning of hPDS STAS domain

All the primers used in this study are shown in Table 1. We initially planned NMR structural characterization of hPDS STAS-ΔIVS using two STAS constructs $hPDS_S$ (aa 512–743) and $hPDS_L$ (aa 512–780) as shown in Fig. 1. Empirical testing of these STAS-ΔIVS constructs revealed low protein yields with high tendency to precipitate during dialysis for imidazole removal (*see below*). In view of the potentially destabilizing role of N-terminal Arg 512 of the above STAS constructs, we generated $hPDS_{ST}$ STAS-ΔIVS constructs in pET-52b(+) and in pET28a(+) (Supplementary Fig. S1) that preserved the predicted secondary structure of the longer constructs (*see* Supplementary Fig. S2).

### 3.2. Expression and isolation of hPDS STAS domain

Growth and induction of *E. coli* expressing STAS-ΔIVS polypeptides $hPDS_L$, $hPDS_S$, and $hPDS_{ST}$ respectively yielded 3.6, 3.3,

**Table 1**
Primer sequences used in PCR amplifications of IVS excluded regions of *hPDS* STAS. Mutagenesis primers #1–5 were to amplify STAS-ΔIVS sequences for cloning $hPDS_{L\ and}$ $hPDS_S$ constructs into pET52b. Primers #6 and 7 were used to shuttle $hPDS_{ST}$ STAS sequence (excluding disordered IVS region) from pET52b(+) into pET-28a(+) for structural studies.

| SLC26A4 STAS | Primer sequence |
|---|---|
| *1. mut_For* | 5′-GACTGTGACCTTGCCATGGCGAGAGTTCAGTTTCCTTCTTGG-3′ |
| *2. mut_Rev* | 5′-GCGTGGCACCAGAGCGAGCTCGGATGCAAGTGTACGCATAGC-3′ |
| *3. mut_Rev-short* | 5′-GCGTGGCACCAGAGCGAGCTCTAAAATGGAACCTTGACCCTC-3′ |
| *4. mutfuse_Rev* | 5′-GCACAAGGCTATGGATTGGCACGGCATCAAATCCAACTGTGGAC-3′ |
| *5. mutfuse_For* | 5′-GTCCACAGTTGGATTTGATGCCGTGCCAATCCATAGCCTTGTGC-3′ |
| *6. 28a_For* | 5′-TCACATATGGCTAGCTCTTGGAATGGCCTTGGAAGC-3′ |
| *7. 28a_Rev* | 5′-CAGGAGCTCGAATTCCTAACCCTCTTGAGATTTCACTTG-3′ |

and 3.3 g wet cell paste per liter culture. SDS-PAGE revealed bands of expected size (in kDa) for hPDS$_L$ (24.3), hPDS$_S$ (20.1) (data not shown), and for hPDS$_{ST}$ (18.8; Fig. 2A). Protein induction was more efficient at 13 °C than at 25 °C or 37 °C. Polypeptide products of each construct partitioned 95% into the insoluble fraction.

Inclusion body lysates were bound to Ni-NTA beads, and eluted with imidazole step gradients. Yields of eluted of STAS-ΔIVS polypeptide were 28% for hPDS$_L$, 21% for hPDS$_S$, and 53% hPDS$_{ST}$. The larger imidazole-resistant retained fractions of STAS-ΔIVS constructs *h*PDS$_L$ and *h*PDS$_S$ were not released even upon addition of ~0.1% (w/v) octyl glucoside (OG) or dodecyl maltoside (DM). Moreover, as much as 88% of initially soluble Ni-NTA-purified STAS-ΔIVS constructs hPDS$_L$ and hPDS$_S$ precipitated during dialysis. The remaining soluble protein was too unstable to allow completion of CD experiments. Purification in buffers containing OG or DM marginally improved protein yield, but CD spectra of these preparations revealed absence of well-folded protein (not shown). We therefore focused subsequent efforts on purification

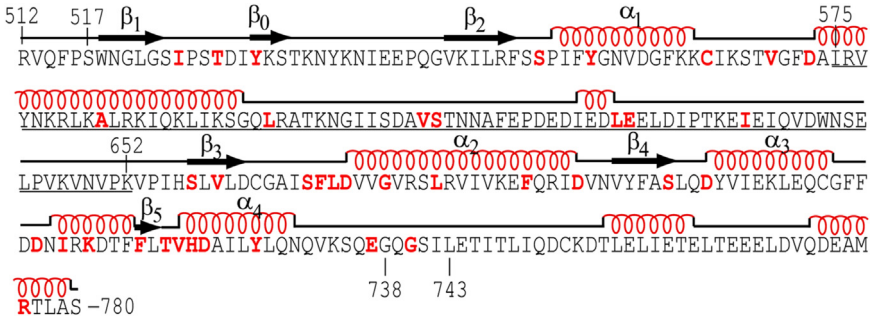


**Fig. 1.** Amino acid (aa) sequence encoded by SLC26A4/hPDS STAS domain cDNA used for molecular cloning and protein expression. Highlighted in red are sites of disease-associated missense mutations. Underlined aa sequence corresponds to the structurally uncharacterized IVS region (aa 575–652), believed to be disordered.

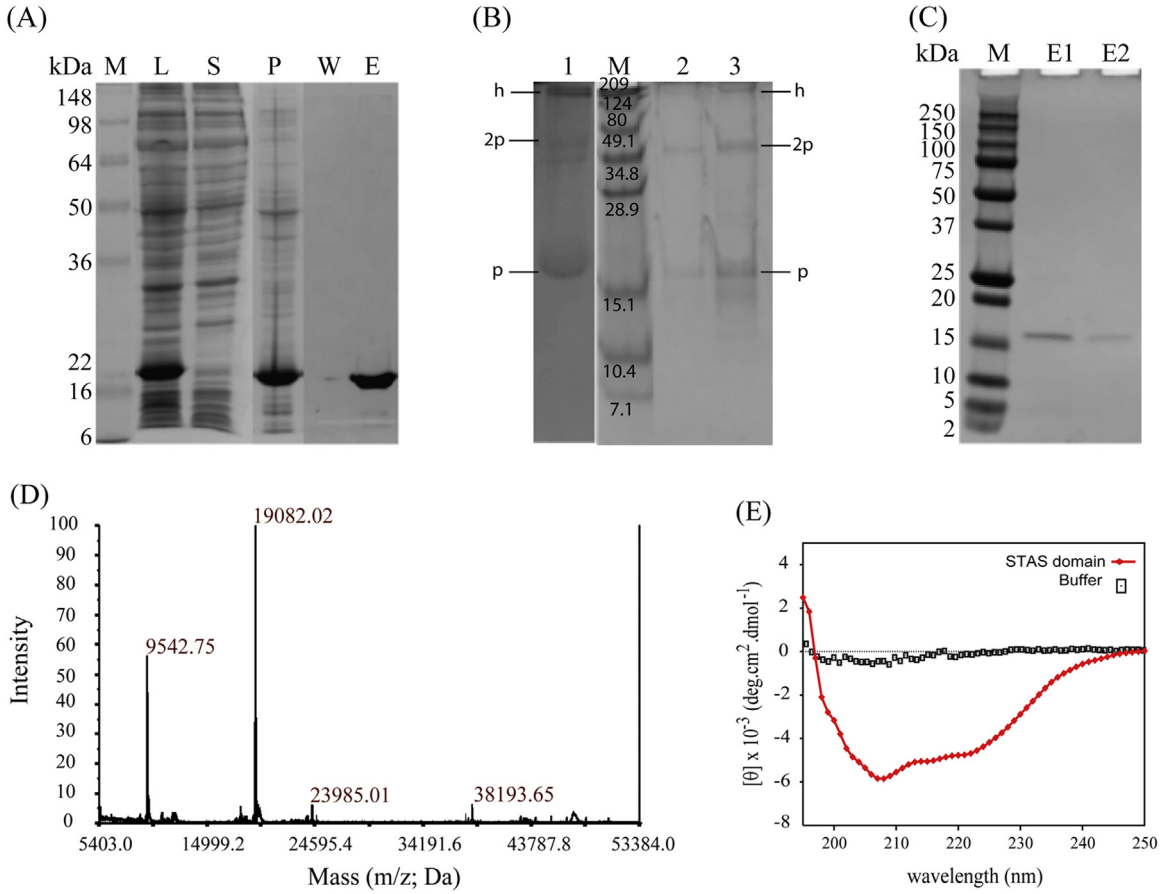


**Fig. 2.** Protein expression and purification, mass and CD spectra of hPDS$_{ST}$ STAS-ΔIVS. Construct includes N-terminal (His)$_6$-tag. (A) Coomassie blue-stained SDS–PAGE (12% w/v) in the presence of 50 mM DTT; Lane M, protein standards; lane L, Lysate post-IPTG induction at 13 °C; lane S, supernatant fraction after centrifugation at 17,000 rpm, 4 °C, 1hr; lane P, insoluble (pellet) fraction after centrifugation; lane W, wash fraction from STAS-bound Ni-NTA beads; lane E, STAS-ΔIVS eluted from Ni-NTA by 500 mM Imidazole in 500 mM NaCl). (B) Immunoblot showing protein monomer (p), dimer (2p), and higher order oligomer bands (h) in lane 1. Size exclusion chromatography fractions in the absence of reducing agent (lanes 2 and 3) show a similar pattern (band labeling similar to lane 1 on 16% w/v SDS-PAGE). (C) hPDS$_{ST}$ STAS-ΔIVS in 1 M NaCl fractionated by anion exchange chromatography and separated in the presence of 50 mM DTT on SDS–PAGE (4–20% w/v), then Coomassie blue-stained. Lane M, protein standards; Lanes E1&E2, eluate fractions. (D) Mass spectroscopic chromatogram shows 19.1 kDa monomer peak of His$_6$-hPDS$_{ST}$ STAS-ΔIVS and 38.2 kDa dimer peak as $K^+$-adducts. A doubly charged species near 9.5 kDa is also seen. Additional peaks of higher mass may represent aggregates. (E) Far-UV CD spectrum of hPDS$_{ST}$ STAS-ΔIVS at 25 °C.

and characterization of $hPDS_{ST}$ STAS-ΔIVS (see Supplementary Table. S1). All the data presented below are from this construct.

Immunoblot of samples in near physiologic salt concentration demonstrated both monomeric and dimeric forms of $hPDS_{ST}$ STAS-ΔIVS (Fig. 2B), with some higher order oligomers. $hPDS_{ST}$ STAS-ΔIVS exhibited less precipitation during dialysis ( $<23\%$) than did larger STAS-ΔIVS polypeptides. Size exclusion chromatography revealed oligomeric forms of protein in solution, corroborating the immunoblot data.

Protein fractionated by size exclusion chromatography was subjected to dialysis for subsequent anion exchange chromatographic purification, with $<7\%$ precipitation during dialysis. Reducing SDS-PAGE of 1 M NaCl eluates from anion exchange chromatography revealed only monomers, suggesting that high salt can shift the conformational equilibrium towards the monomeric state (Fig. 2C). Reducing [NaCl] to $\leq 150$ mM restored oligomeric heterogeneity. Maintaining [NaCl] $\geq 500$ mM reliably reduced oligomerization of $hPDS_{ST}$ STAS-ΔIVS.

### 3.3. Yields of His6-tag-free STAS $hPDS_{ST}$ polypeptide

$His_6$ tag removal from the STAS-ΔIVS polypeptides led to major protein loss ( $<25\%$ recovery). Tag-free samples exhibited moderate precipitation at later stages of purification, and resulting sample quantities were insufficient for 1D $^1H$ NMR studies. Therefore, further attempts to optimize purification of His-tag-free STAS-ΔIVS polypeptides were discontinued.

### 3.4. MALDI-TOF MS

Mass spectrometry of $hPDS_{ST}$ STAS in buffers lacking reducing agent was not successful. Data collected in sample buffers containing $\geq$ 9 mM tris-carboxyethylphosphine resulted in mass detection of potassiated monomeric and dimeric species of protein (Fig. 2D), accompanied by 2 forms of uncertain oligomeric stoichiometry.

### 3.5. CD spectroscopy

Fig. 2E shows the CD spectrum of $hPDS_{ST}$ STAS-ΔIVS. The data show secondary structural elements suggesting a folded conformation in solution. The characteristic double ellipticity minima at 208 and 220 nm are diagnostic for helical structure. The spectral lineshape pattern, including the noted ellipticity differences at the two minima, shows the presence of β-strand structure. Spectral deconvolution analysis predicts that secondary structural elements constitute ~41% of the polypeptide. Correcting for the His6-fusion tag at the N-terminus, the measured % secondary structure is close to that predicted (~ 46%) from the $hPDS_{ST}$ STAS-ΔIVS model built on the rat prestin STAS-ΔIVS template. These results show that purified, recombinant $hPDS_{ST}$ STAS-ΔIVS polypeptide refolded from inclusion body lysate adopts a well folded, structured conformation in solution.

### 3.6. NMR spectroscopy of $hPDS_{ST}$ STAS domain

The folded state of hPDS STAS was further examined by applying 1D $^1H$ and 2D heteronuclear solution NMR methods (Fig. 3). First we attempted 2D $^1H$–$^{15}N$ HSQC spectra on the $hPDS_{ST}$ STAS-ΔIVS sample in buffer C, pH 7.9 (as used for CD measurements). Although the data showed good dispersion of $^1H$–$^{15}N$ correlation crosspeaks of weak intensity on a directly detected dimension, the observed number of $^1H$–$^{15}N$ backbone correlation crosspeaks in the 2D $^1H$–$^{15}N$ HSQC spectrum was less than half the expected 140 non-proline residues (see Fig. S1 *for aa sequence of* $STAS_{ST}$-ΔIVS), likely due to amide proton exchange with solvent and/or to the

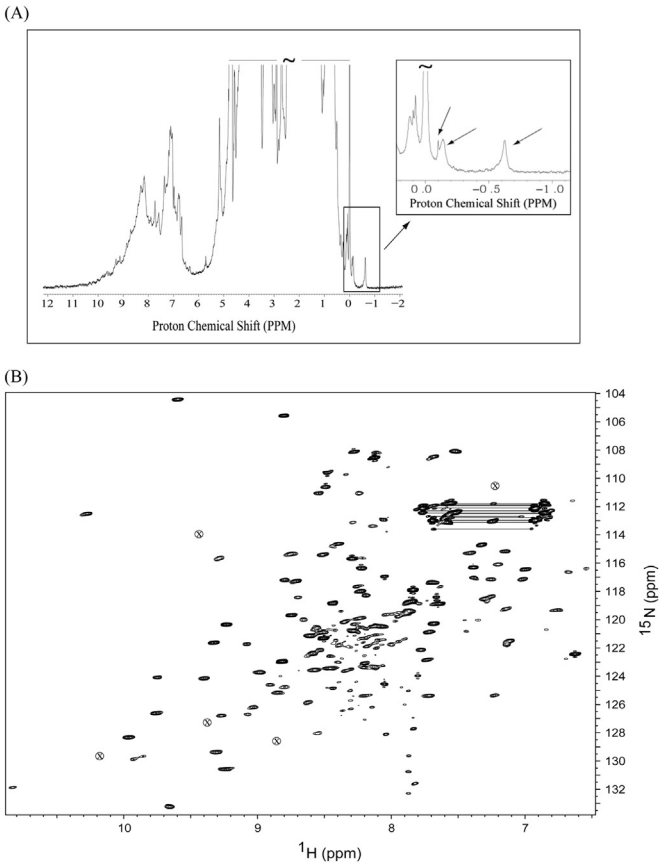


**Fig. 3.** (A) One-dimensional NMR spectrum of a uniformly $^{15}N$-enriched sample of $hPDS_{ST}$ STAS-ΔIVS. The proton signals above 9.0 ppm and below 0.5 ppm indicate protein in a compact folded state. Methyl proton signals below 0.0 ppm likely reflect ring current effect (arising from interaction with aromatic ring protons), further supporting the folded state in these solution conditions. Inset shows magnified region of methyl peaks below 0.0 ppm. (B) Heteronuclear two-dimensional $^1H$–$^{15}N$ HSQC spectrum of $hPDS_{ST}$ STAS-ΔIVS. The 5 additional crosspeaks seen at higher contour level are highlighted as circled X's. Horizontal lines connect side chain $^1H$–$^{15}N$ correlation crosspeaks arising from Asn and Gln residues.

presence of higher order STAS-ΔIVS oligomers in solution. The results nonetheless suggested a folded state for purified protein in this condition. Empiric assessment of buffer pH-dependence of STAS-ΔIVS stability in solution led to subsequent NMR data collection at pH 6.2.

One-dimensional $^1H$ NMR spectrum dispersion of ~10.80–6.50 ppm clearly demonstrates a folded conformation of $hPDS_{ST}$ STAS-ΔIVS in solution (Fig. 3A). The moderately sharper linewidths of most peaks within the backbone amide region suggests the likely predominance of monomeric protein. The few peaks at 4.5–6.0 ppm likely correspond to $^1H^{\alpha}$ resonances of residues constituting β-strand structures in the protein structure fold, corroborating the CD data. Select $^1H$ peaks below 0.0 ppm probably represent methyl proton peaks of residues experiencing a ring current shift due to interaction with aromatic residue ring protons within the tertiary structural fold (region magnified in Inset). These parameters show that $hPDS_{ST}$ STAS-ΔIVS is well-folded, with regions of tertiary structure.

The 2D $^1H$–$^{15}N$ HSQC spectrum of STAS-ΔIVS (Fig. 3B) shows at least one $^1H$–$^{15}N$ backbone correlation crosspeak for most of the polypeptide's non-proline amino acid residues. The $^1H$–$^{15}N$ side-chain correlations from Asn, Gln, and Trp residues are also evident in the spectrum. The chemical shift dispersion of these correlation crosspeaks for a well-folded STAS domain may exhibit a dispersed $^1H$ ppm spectral window (Fig. 3B), which for an intrinsically disordered or unfolded/partially folded protein would shrink to a

narrow ppm window (~8.6–7.0 ppm). The highly resolved $^{1}H$–$^{15}N$ HSQC spectrum (10.3 h acquizition at pH 6.2) shown in Fig. 3B exhibits 151 cross-peaks (excluding the side-chain correlations) and excellent chemical shift dispersion of 10.83–6.57 $^{1}H$ ppm. Five additional backbone $^{1}H^{N}$ correlations crosspeaks of higher contour are also evident (circled X's in Fig. 3B). The $^{1}H$–$^{15}N$ HSQC spectra recorded at shorter acquizition time (Supplementary Table S3) shows complete crosspeak dispersion similar to that of the longer acquizition time spectrum. Maintenance of spectral quality during 1 week of sample storage suggests stability of protein conformation at 0.25 mM during this time.

The expected number of $^{1}H$–$^{15}N$ backbone correlation crosspeaks for this construct (Fig. S1) is 162, including 23 $^{1}H$–$^{15}N$ correlation crosspeaks predicted to arise from the N-terminal cleavable $(His)_6$-fusion tag. The 156 crosspeaks detected in the spectrum likely include all or most core protein resonances. Two sets of crosspeaks of different intensity distributions were present in the spectrum. The predominant set of ~130 crosspeaks shows moderately sharper linewidths, whereas, the minority set of ~26 crosspeaks has broader linewidths of intensity at least 50% lower than the average intensity of the majority set of crosspeaks. These differences in linewidth might reflect different dynamic properties elicited by the respective resonances. The weaker intensity crosspeaks could include some or all $^{1}H$–$^{15}N$ resonances from the (unstructured) $(His)_6$ tag region, and/or could reflect solvent exchange effects for these $^{1}H^{N}$ resonances. Although protein aggregation was operationally minimized at pH 6.2, a degree of oligomerization producing slower rotational correlation times of minority set of crosspeaks cannot be ruled out. Future completion of NMR assignment will provide further details.

Fig. 4 shows the well-dispersed 2D $^{1}H$–$^{13}C$ HSQC spectrum of $hPDS_{ST}$ STAS-ΔIVS. Downfield-shifted $^{1}H$–$^{13}C$ correlation crosspeaks within the $^{1}H^{\alpha}$ region likely indicate signals from residues involved in β-strand formation. The extreme upfield-shifted crosspeaks (below 0.0 ppm) identify residues likely exhibiting a ring current shift effect, corroborating the 1D $^{1}H$ NMR data. These data together suggest that $hPDS_{ST}$ STAS-ΔIVS adopts a folded conformation in solution.

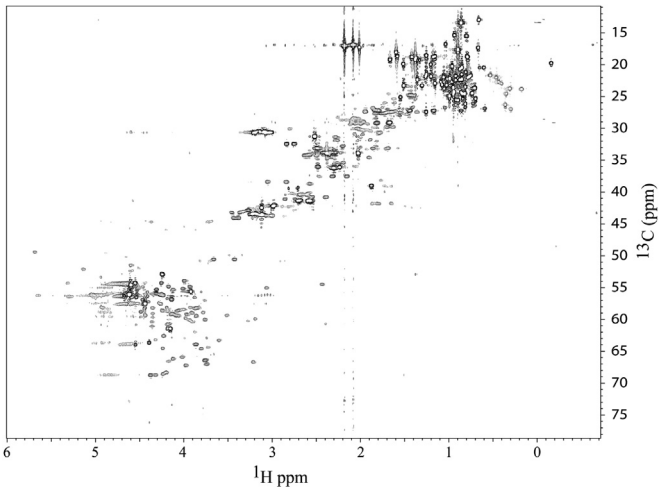


**Fig. 4.** Heteronuclear 2D $^{1}H$–$^{13}C$ HSQC spectrum of $hPDS_{ST}$ STAS-ΔIVS. $^{1}H$–$^{13}C$ correlation crosspeaks are well-dispersed. Downfield shifted $^{1}H$–$^{13}C$ correlation crosspeaks within $^{1}H^{\alpha}$ region likely indicate signals from residues involved in β-strand formation. The extreme upfield-shifted crosspeaks (below 0.0 ppm) likely identify residues exhibiting ring current shift effect, and corroborate the 1D $^{1}H$ NMR data presented here.

### 3.7. NMR detection of nucleotide binding by $hPDS_{ST}$ STAS

The nucleotide-binding properties of anti-σ factor antagonist SpoIIAA [27], STAS domain of Rv1739c from *M. tuberculosis* [15], and STAS domains from full-length YchM/DauA [12] prompted evaluation of nucleotide binding by $hPDS_{ST}$ STAS-ΔIVS.

We first tested stability of NMR samples by collecting a series of 2D $^{1}H$–$^{15}N$ HSQCs (2 h 45 min each) at days 1, 3, 4, and 7 after purification, with storage at 4 °C. All 2D $^{1}H$–$^{15}N$ HSQC spectra revealed similar degrees of dispersion, with minimal precipitation over the 7 d period. These data warranted preparation of $^{13}C/^{15}N$ doubly-enriched NMR sample for resonance assignment and structural characterization.

In order to study $hPDS_{ST}$ STAS-ΔIVS interaction with nucleotide by NMR chemical shift perturbation (CSP), 2D $^{1}H$–$^{15}N$ HSQC spectra of freshly prepared $^{15}N$-STAS-ΔIVS were collected in the presence of sequentially increasing [GDP]. Data revealed GDP-induced NMR chemical shift perturbation (CSP) for select protein residues. NMR titration experiments identified 20 mM GDP as a saturating concentration for hPDS STAS-ΔIVS, as higher concentrations did not significantly increase CSP (not shown). Overlay of 2D $^{1}H$–$^{15}N$ HSQC spectra of STAS-ΔIVS domain in the absence and presence of increasing [GDP] is shown in Fig. 5A. Sections of the spectrum with residues exhibiting the largest GDP-induced CSPs are enlarged in Fig. 5B–D. GDP-induced conformational perturbations include resonances showing only weighted average peak shifts, whereas other select resonances exhibit peak shifts accompanied by decreased crosspeak intensity. GDP addition to STAS-ΔIVS also elicited emergence of several novel resonances (Fig. 5A and B) probably reflecting nucleotide-induced stabilization of normally undetected, flexible residues, and/or slow conformational exchange of select residues in their local environments. These analyses suggest that GDP binding induces CSP of select protein residues, a process that occurs at faster-intermediate NMR time scales. Taken together, these results strongly suggest that $hPDS_{ST}$ STAS-ΔIVS binds guanine nucleotide.

### 3.8. Nucleotide binding by $hPDS_{ST}$ STAS-ΔIVS by intrinsic fluorescence quench

The presence in $hPDS_{ST}$ STAS-ΔIVS (Fig. 1) of a single Trp residue, Trp518, and 6 Tyr residues (Tyr530, Tyr536, Tyr556, Tyr691, Tyr698, and Tyr728) allowed assessment of nucleotide binding by intrinsic fluorescence quench. $hPDS_{ST}$ subjected to 280 nm excitation exhibited a fluorescence emission $\lambda_{max}$ of 320 nm. Fig. 6A illustrates the gradual quench of intrinsic STAS fluorescence with progressively increasing concentrations of GDP, with maximum observed quench of 14.2%. The observed quench isotherm is compatible with a single nucleotide binding site of $K_{1/2} = 178 \pm 81$ μM (Fig. 6B). The data suggest a nucleotide interaction surface in STAS domain that directly or indirectly perturbs Trp and/or Tyr residues through conformational effects on adjacent or interposed residues. These results are consistent with the heteronuclear NMR data showing nucleotide binding by $hPDS_{ST}$ STAS-ΔIVS. Similar future experiments will examine nucleotide binding of full-length wild type and disease-associated mutants, and define the nucleotide binding surface of the protein. Preliminary data (Sharma et al., unpublished) confirm nucleotide binding by the recombinant full-length STAS domain of *A. thaliana* sulfate transporter SULTR1;2, further strengthening the hypothesis that STAS domains are nucleotide binding proteins [4].

The tendency of $hPDS_{ST}$ STAS-ΔIVS to aggregate was modulated by salt concentration and pH. Buffer conditions of ≥ 500 mM NaCl and pH 6.2 each reduced protein aggregation. At 150 mM NaCl, the protein exhibited a similar monomer-dimer equilibrium at both pH 6.2 and pH 7.9. SLC26A/SulP proteins in solution are known to exhibit dimeric and higher order oligomeric structures [2,12,28]. Rat

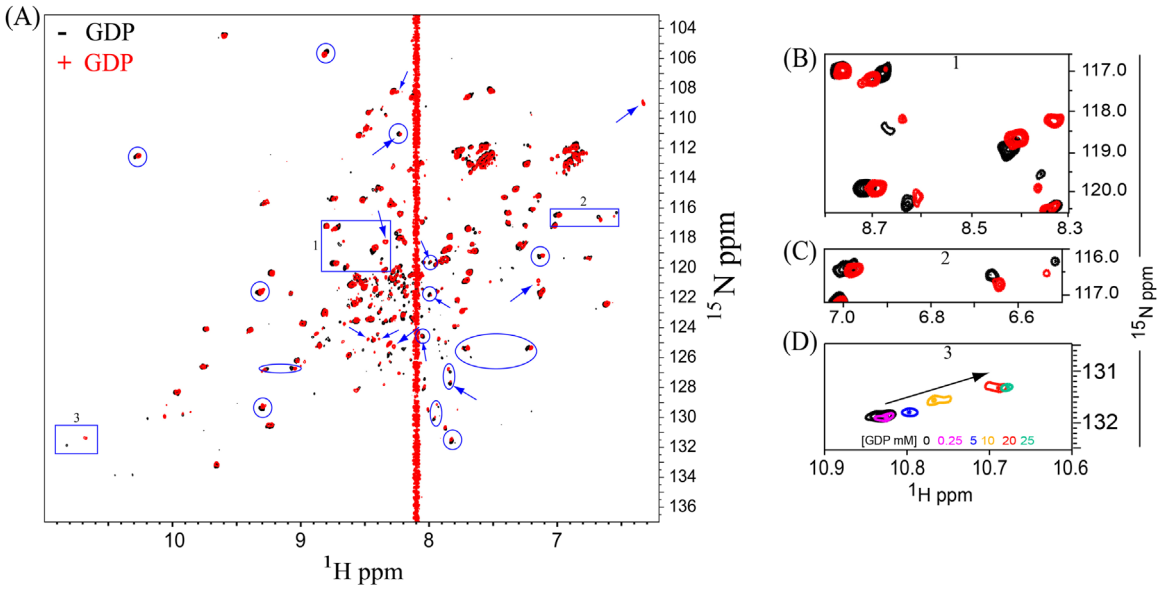


**Fig. 5.** NMR detection of GDP interactions with $hPDS_{ST}$ STAS-ΔIVS. (A) Superposition of 2D $^{1}$H–$^{15}$N HSQC spectra of hPDS STAS in absence (black contours) and presence of 20 mM GDP (red contours). Chemically perturbed $^{1}$H–$^{15}$N correlation resonances are indicated by circles, ellipses, and boxes. Arrows show emergent resonances in GDP-saturated STAS spectra. Arrowed circles denote resonances showing CSP with decreased intensity. The guanine proton peak is at ~8.09 ppm. (B and C) Magnified regions of boxed portions of 2D $^{1}$H–$^{15}$N HSQC of STAS-ΔIVS in absence (black) and presence of (saturating) 20 mM GDP (red). (D) Tryptophan side-chain $^{1}$H–$^{15}$N correlation crosspeaks showing graded perturbation upon titration with increasing [GDP] (scale below panel).

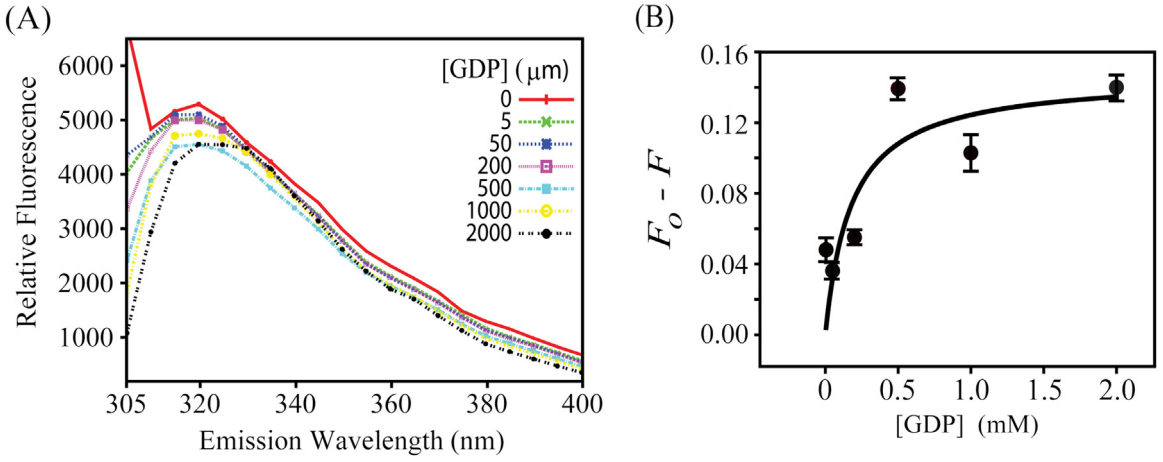


**Fig. 6.** Intrinsic tryptophan/tyrosine fluorescence quench (A) Intrinsic fluorescence quench of $hPDS_{ST}$ STAS-ΔIVS (20–23 μM) by indicated [GDP]. (B) GDP concentration dependence for quench of $hPDS_{ST}$ STAS peak intrinsic fluorescence at 320 nm, with $K_{1/2} = 178 \pm 81$ μM. Values are mean ± S.E. ($n = 3$).

Prestin STAS-ΔIVS exhibited dimers and tetramers in solution with a tendency toward formation of higher molecular weight aggregates [29]. Recombinant mouse Slc26a9 STAS also exhibited a monomer-dimer equilibrium [30]. Protein aggregation was noted for *E. coli* DauA STAS domain variants harboring mutations at the sites homologous to the disease-associated mutations in SLC26 STAS domains [31]. Future studies will test the role of the three Cys residues of hPDS STAS (aa 565, 662, and 706) in STAS oligomerization. Rat prestin STAS template-based modeling of hPDS STAS-ΔIVS suggests occupancy of flexible loop positions by the three homologous Cys residues (Cys706 is the first residue in helix α3) with side chain exposure to the solvent environment (Supplementary Fig. S4). Thus, alterations in solvent pH, salt concentration, and redox environment may influence the native cysteine-cystine equilibrium, including possible inter-monomer cystine linkage.

IVS deletion from the hPDS STAS domain has allowed a reproducible purification protocol, yielding well-folded protein in quantities suitable for NMR structural studies. Attempts are currently underway to purify full-length hPDS STAS domain polypeptide from soluble fractions in quantity sufficient for solution NMR, using solubility-enhancing fusion tags. However, the present study shows that the IVS region is dispensable for nucleotide binding by hPDS STAS.

## 4. Conclusions

The class of eukaryotic STAS domains from rodent and human SLC26 transporters has proven difficult to express in a well-folded conformation at the high concentrations required for structural studies. With the exception of rat SLC26A5/prestin, only one $^{1}$H–$^{15}$N 2D HSQC spectrum has been reported from a mammalian STAS domain (SLC26A3). However no structural information has been reported for SLC26A3 STAS domain, perhaps reflecting low sample solubility [8], or for STAS domain from any human member. Here we have

presented data on the molecular cloning, expression and purification, and protein folding characterization of $hPDS_{ST}$ STAS-ΔIVS as characterized by CD and by 1D and 2D heteronuclear NMR. Our purification protocol has yielded well-folded U-$^{13}C/^{15}N$ labeled recombinant STAS in the milligram quantities sufficient for future unambiguous NMR residue assignment and elucidation of three dimensional structure of this deafness gene product, SLC26A4/pendrin. We found that $hPDS_{ST}$ STAS-ΔIVS exists in solution in monomer and dimer states, with propensity to higher-order oligomerization. We showed by intrinsic fluorescence quench and by CSP NMR methods that hPDS STAS-ΔIVS can bind GDP. These results are of importance not only for structure/function studies of hPDS STAS, but may in addition be applicable to STAS domains of other human SLC26 anion transporter polypeptides. This information will increase our understanding of a known therapeutic target for treatment of congenital deafness. It will also increase understanding of an underappreciated major pathway for distal nephron chloride reabsorption representing an important target for diuretic development, with implications for enhanced management of fluid overload in settings of trauma and intensive care, and in chronic cardiac, renal, and liver diseases.

## Funding sources

This work was supported by NIDDK Grants R01-43495 (SLA) and P30-DK34854 (Harvard Digestive Diseases Center to SLA) and by US-Israel Binational Science Foundation Grant 2009129 (IZ and SLA).

## Conflict of interest

The authors declare no conflicts of interest.

## Acknowledgments

We thank Gonen Memisoglu (Brandeis University, Waltham, MA) for assistance with protein purification, and Prof. Martin R. Pollak for support. Authors acknowledge Ananya A. Sharma for her support during revision of this manuscript. All NMR data were collected at The Biological NMR Center, Tufts University, Boston on a Bruker Avance 600 MHz.

## Appendix A. Transparency document

Transparency document data associated with this article can be found in the online version at http://dx.doi.org/10.1016/j.bbrep.2016.08.022.

## Appendix B. Supplementary material

Supplementary data associated with this article can be found in the online version at http://dx.doi.org/10.1016/j.bbrep.2016.08.022.

## References

[1] J. Felce, M.H. Saier Jr., Carbonic anhydrases fused to anion transporters of the SulP family: evidence for a novel type of bicarbonate transporter, J. Mol. Microbiol. Biotechnol. 8 (2004) 169–176.
[2] S.L. Alper, A.K. Sharma, The SLC26 gene family of anion transporters and channels, Mol. Asp. Med. 34 (2013) 494–515.
[3] E.R. Geertsma, Y.N. Chang, F.R. Shaik, Y. Neldner, E. Pardon, J. Steyaert, R. Dutzler, Structure of a prokaryotic fumarate transporter reveals the architecture of the SLC26 family, Nat. Struct. Mol. Biol. 22 (2015) 803–808.
[4] L. Aravind, E.V. Koonin, The STAS domain - a link between anion transporters and antisigma-factor antagonists, Curr. Biol. 10 (2000) R53–R55.
[5] A.K. Sharma, A.C. Rigby, S.L. Alper, STAS domain structure and function, Cell Physiol. Biochem. 28 (2011) 407–422.
[6] S. Masuda, K.S. Murakami, S. Wang, C. Anders Olson, J. Donigian, F. Leon, S. A. Darst, E.A. Campbell, Crystal structures of the ADP and ATP bound forms of the Bacillus anti-sigma factor SpoIIAB in complex with the anti-anti-sigma SpoIIAA, J. Mol. Biol. 340 (2004) 941–956.
[7] M.N. Chernova, L. Jiang, B.E. Shmukler, C.W. Schweinfest, P. Blanco, S. D. Freedman, A.K. Stewart, S.L. Alper, Acute regulation of the SLC26A3 congenital chloride diarrhoea anion exchanger (DRA) expressed in Xenopus oocytes, J. Physiol. 549 (2003) 3–19.
[8] M.R. Dorwart, N. Shcheynikov, J.M. Baker, J.D. Forman-Kay, S. Muallem, P. J. Thomas, Congenital chloride-losing diarrhea causing mutations in the STAS domain result in misfolding and mistrafficking of SLC26A3, J. Biol. Chem. 283 (2008) 8711–8722.
[9] M.R. Dorwart, N. Shcheynikov, D. Yang, S. Muallem, The solute carrier 26 family of proteins in epithelial ion transport, Physiology 23 (2008) 104–114.
[10] S. Dossena, E. Bernardinelli, A.K. Sharma, S.L. Alper, M. Paulmichl, The Pendrin Polypeptide Springer, 2016 (in press).
[11] E. Karinou, E.L. Compton, M. Morel, A. Javelle, The Escherichia coli SLC26 homologue YchM (DauA) is a C(4)-dicarboxylic acid transporter, Mol. Microbiol. 87 (2013) 623–640.
[12] L. Srinivasan, T.L. Baars, K. Fendler, H. Michel, Functional characterization of solute carrier (SLC) 26/sulfate permease (SulP) proteins in membrane mimetic systems, Biochim. Biophys. Acta 1858 (2016) 698–705.
[13] G.J. Babu M, A. Emili, N.C. Strynadka, R.A. Reithmeier, T.F. Moraes, Structure of a SLC26 anion transporter STAS domain in complex with acyl carrier protein: implications for E. coli YchM in fatty acid metabolism, Structure 18 (2010) 1450–1462.
[14] E. Pasqualetto, R. Aiello, L. Gesiot, G. Bonetto, M. Bellanda, R. Battistutta, Structure of the cytosolic portion of the motor protein prestin and functional role of the STAS domain in SLC26/SulP anion transporters, J. Mol. Biol. 400 (2010) 448–462.
[15] A.K. Sharma, L. Ye, C.E. Baer, K. Shanmugasundaram, T. Alber, S.L. Alper, A. C. Rigby, Solution structure of the guanine nucleotide-binding STAS domain of SLC26-related SulP protein Rv1739c from Mycobacterium tuberculosis, J. Biol. Chem. 286 (2011) 8534–8544.
[16] N. Shibagaki, A.R. Grossman, Binding of cysteine synthase to the STAS domain of sulfate transporter and its regulatory consequences, J. Biol. Chem. 285 (2010) 25094–25102.
[17] A.K. Sharma, I. Zelikovic, S.L. Alper, Molecular dynamics simulations of the STAS Domains of rat prestin and human pendrin reveal conformational motions in conserved flexible regions, Cell. Physiol. Biochem. 33 (2014) 605–620.
[18] A.K. Sharma, L. Ye, A.S. Zolotarev, S.L. Alper, A.C. Rigby, NMR assignment and secondary structure of the STAS domain of Rv1739c, a putative sulfate transporter of Mycobacterium tuberculosis, Biomol. NMR Assign. 3 (2009) 99–102.
[19] M.M. Bradford, A rapid and sensitive method for the quantitation of microgram quantities of protein utilizing the principle of protein-dye binding, Anal. Biochem. 72 (1976) 248–254.
[20] C. Perez-Iratxeta, M.A. Andrade-Navarro, K2D2: estimation of protein secondary structure from circular dichroism spectra, BMC Struct. Biol. 8 (2008) 25.
[21] S. Mori, C. Abeygunawardana, M.O. Johnson, P.C. van Zijl, Improved sensitivity of HSQC spectra of exchanging protons at short interscan delays using a new fast HSQC (FHSQC) detection scheme that avoids water saturation, J. Magn. Reson. B 108 (1995) 94–98.
[22] G.W.B. Vuister, A. Resolution, enhancement and spectral editing of uniformly 13C-enriched proteins by homonuclear broadband 13C decoupling, J. Magn. Reson. 98 (1992) 428–435.
[23] F. Delaglio, S. Grzesiek, G.W. Vuister, G. Zhu, J. Pfeifer, A. Bax, NMRPipe: a multidimensional spectral processing system based on UNIX pipes, J. Biomol. NMR 6 (1995) 277–293.
[24] D.S.B. Wishart, C G, J. Yao, F. Abildgaard, H.J. Dyson, E. Oldfield, J.L. Markley, B. D. Sykes, 1 H, 13C and 15N chemical shift referencing in biomolecular NMR, J. Biomol. NMR 6 (1995) 135–140.
[25] W.F. Vranken, W. Boucher, T.J. Stevens, R.H. Fogh, A. Pajon, M. Llinas, E.L. Ulrich, J. L. Markley, J. Ionides, E.D. Laue, The CCPN data model for NMR spectroscopy: development of a software pipeline, Proteins 59 (2005) 687–696.
[26] A. Rao, P. Martin, R.A. Reithmeier, L.C. Cantley, Location of the stilbenedisulfonate binding site of the human erythrocyte anion-exchange system by resonance energy transfer, Biochemistry 18 (1979) 4505–4516.
[27] S.M. Najafi, D.A. Harris, M.D. Yudkin, The SpoIIAA protein of Bacillus subtilis has GTP-binding properties, J. Bacteriol. 178 (1996) 6632–6634.
[28] E.L. Compton, K. Page, H.E. Findlay, M. Haertlein, M. Moulin, U. Zachariae, D. G. Norman, F. Gabel, A. Javelle, Conserved structure and domain organization among bacterial Slc26 transporters, Biochem. J. 463 (2014) 0297–0307.
[29] E. Pasqualetto, A. Seydel, A. Pellini, R. Battistutta, Expression, purification and characterisation of the C-terminal STAS domain of the SLC26 anion transporter prestin, Protein Expr. Purif. 58 (2008) 249–256.
[30] M.H. Chang, C. Plata, A. Sindic, W.K. Ranatunga, A.P. Chen, K. Zandi-Nejad, K. W. Chan, J. Thompson, D.B. Mount, M.F. Romero, Slc26a9 is inhibited by the R-region of the cystic fibrosis transmembrane conductance regulator via the STAS domain, J. Biol. Chem. 284 (2009) 28306–28318.
[31] X. Bai, T.F. Moraes, R.A. Reithmeier, Effect of SLC26 anion transporter disease-causing mutations on the stability of the homologous STAS domain of E. coli DauA (YchM), Biochem. J. 473 (2016) 615–626.